RSC Advances

ROYAL SOCIETY OF CHEMISTRY

www.rsc.org/advances

RSC Advances

ARTICLE

Flexible Additive-Free CC@TiO_xN_y@SnS_2 Nanocomposites with Excellent Stability and Superior Rate Capability for Lithium Ion Batteries

Received 00th January 20xx,
Accepted 00th January 20xx

DOI: 10.1039/x0xx00000x

www.rsc.org/

Fengqi Lu, *[a] Qiang Chen,[a] Yibin Wang,[a] Yonghao Wu,[a] Pengcheng Wei[a]nd Xiaojun Kuang[a]

A novel material consisting of metal oxide-nitride (TiO_xN_y nanowires) and metal sulfide (SnS_2 nanosheets) is synthesized on a flexible carbon cloth substrate by two steps hydrothermal reaction. The as-synthesized carbon cloths/titanium oxynitride/tin disulfide (CC@TiO_xN_y@SnS_2) nanocomposites are tested directly as additive-free anode materials for lithium-ion batteries. The free-standing CC@TiO_xN_y@SnS_2 electrode displays an initial discharge capacity of 1082 mAh g^{-1} at a current density of 1 C, with a coulombic efficiency of 74 %. The reversible capacity as high as 612 mAh g^{-1} can still be maintained after 100 charging/discharging cycles. Moreover, this material shows outstanding rate property with a high reversible discharge capacity of 419 mAh g^{-1} at a current density of 5 C, which is higher than the theory capacity of graphite. Also, a stable high discharge capacity of 676 mAh g^{-1} can be attained when the current density is switched back to 1 C. The high electrochemical performance can be attributed to the high electrical conductivity of the TiO_xN_y facilitates the transport of electrons and lithium ions and the unique layer structure of SnS_2.

1. Introduction

Lithium-ion batteries (LIBs) bear with many superior properties, including high energy and power densities, long cycle life, and environmental benignity, and thus have been regarded as ideal power supplies for electric vehicles (EVs) and hybrid electric vehicles (HEVs).[1, 2] To fulfill the increasing demands for HEVs and EVs practicable applications, LIBs with higher energy, larger powder and longer cycle lifespan are highly required. Unfortunately, commercially used graphite carbon has struggled to meet these requirements because of its low theoretical capacity (~372 mAh g^{-1}).[3]

To date, various materials have been developed as promising high performance anode electrodes of LIBs.[4-8] Among of them, tin disulfides (SnS_2) has received considerable attention due to its high theoretical capacity.[9-15] SnS_2 has a layered CdI_2-type structure, in which tin atoms are sandwiched two layers of sulfur atoms. Recent studies have shown that nanostructured SnS_2-base materials revealed that remarkably improved electrochemical properties as anode material for LIBs compared to their bulk counterparts, which primarily owns to their unique morphology, consist of a finite lateral sized and its well-defined layered structure. For example, acetylene black incorporated porous 3-dimensional (3D) SnS_2 nanoflowers show high cyclability and rate capability and deliver an average reversible capacity as high as 525 mAh g^{-1} at a current density of 400 mA h/g over 70 cycles.[16] Preferential c-Axis orientation of ultrathin SnS_2 nanoplates on graphene can maintain a charge capacity of 704 mAh g^{-1} after 100 cycles at 0.6 C and deliver a charge capacity of 303 mAh g^{-1} at 10 C.[17] Lamellar sandwich SnS_2@PANI nanoplates have a high initial reversible capacity (968.7 mAh g^{-1}), excellent cyclability (730.8 mAh g^{-1} after 80 cycles), and an extraordinary rate capability (356 mAh g^{-1} at the rate of 5A g^{-1}).[18] Free-standing SnS_2@graphene nanocable network not only shows high specific capacity of 720 mAh g^{-1} even after 350 cycles at a current density of 0.2 A g^{-1}, with over 93.5% capacity retention, but also exhibits a high-rate capability of 580 mAh g^{-1} even at the current rate of 1 A g^{-1}.[19] However, its major volume expansion during the charge–discharge process leads to a significant capacity loss and poor cycling stability, which greatly hinders its practical application in lithium-ion batteries. Thus, it is necessary to explore a useful method to improve the reversible capacity and lithium storage performance of SnS_2.

Carbon cloths (CC), a new kind of substrate, have been received large attention because their high conductivity, excellent mechanical flexibility and high strength. They have been utilized as substrate for the growth of electrode materials in order to serve as binder-free, enabling high capacity, good cycling stability and excellent rate performance for flexible LIBs.[20-25] Also, titanium oxynitride (TiO_xN_y) has been reported to be a crucial factor in composite electrodes

Guangxi Ministry-Province Jointly-Constructed Cultivation Base for State Key Laboratory of Processing for Nonferrous Metal and Featured Materials, Guangxi Universities Key Laboratory of Non-ferrous Metal Oxide Electronic Functional Materials and Devices, College of Materials Science and Engineering, Guilin University of Technology, Guilin 541004 P. R. China. Email: lufengqi@glut.edu.cn; Tel: +86 773 5890706.

† Electronic Supplementary Information (ESI) available: XRD Spectra of CC@TiN, CC@TiOxNy@SnS_2, SnS_2 and CC@SnS_2, SEM images of the CC@SnS_2 and SnS_2, Raman Spectrum of CC@TiOxNy@SnS_2, CV profiles and the 1st, 2nd and 100th charging/discharging voltage curves of CC (e), SnS_2 nanosheets (f), CC@SnS_2 (g) and CC@TiN (h) electrode, coulombic efficiency curve of CC@TiOxNy@SnS_2 electrode, SEM images of the CC@TiOxNy@SnS_2 electrode after 100 cycles. See DOI: 10.1039/x0xx00000x.

because they have the merit of high dispersion of the active material in a highly conductive matrix, which would curb the particles aggregation and dramatically boost the cycling performance of LIBs at high charge/discharge rates.[26-29]

Herein, we develop a facile strategy to design and fabricate a unique hierarchical hybrid structure of carbon cloths supported TiO_xN_y and SnS_2 (denoted as CC@TiO_xN_y@SnS_2) as flexible additive-free anode material for LIBs. With the compositional and structure advantages, the as-synthesized CC@TiO_xN_y@SnS_2 electrode display an initial discharge capacity of 1082 mAh g^{-1} at a current density of 1 C, the reversible capacity as high as 612 mAh g^{-1} can still be maintained after 100 charging/discharging cycles. Moreover, these materials show a high reversible discharge capacity of 419 mAh g^{-1} at a current density of 5 C, a stable high discharge capacity of 676 mAh g^{-1} can be attained when the current density is switched back to 1 C.

2. Experimental Method

2.1 Materials

Carbon cloth (flexible substrate), Titanium (IV) tetrachloride ($TiCl_4$, 99%), concentrated hydrochloric acid (HCl, AR), tetrabutyl titanate [$Ti(OC_4H_9)_4$, 98%], Tin chloride pentahydrate ($SnCl_4{\cdot}5H_2O$, AR), L-cysteine ($C_3H_7NO_2S$, AR) and ethanol (C_2H_5OH, AR) were purchased from Chemical Reagents Factory and used without further purification.

2.2 Synthesis of CC@TiN

TiO_2 nanowires were grown on a carbon cloth by hydrothermal method according to the previous report.[30] In a typical procedure, a piece of carbon cloth with 2.5 cm × 4 cm was cleaned with deionized water, ethanol, sequentially for 30 minutes in an ultrasonic bath, respectively, and then dried at room temperature. The cleaned carbon cloth was immersed in 0.2 M aqueous titanium (IV) tetrachloride solution for two minutes and allowed to be dried by blowing in the compressed air. And then the blown-dried carbon cloth was heated on a hotplate at about 320 ^oC for few minutes, which generated nanoparticles on the surface of the carbon cloths. This process was repeated about four times to ensure uniformity. 20 mL of concentrated hydrogen chloride acid was diluted in 20 mL deionized water and then mixed with 1.2 mL of tetrabutyl titanate under stirring on a magnetic stirrer until a clear solution was obtained. The carbon cloth was then immersed in the clear solution and transferred to Teflon-lined stainless steel autoclave (50 mL). The sealed autoclave was heated in an electric oven at 160 ^oC for 330 minutes and cooled down to room temperature. The carbon cloths with TiO_2 samples was washed thoroughly with deionized water several times and dried in air. To obtain the TiN nanowires, the synthesized TiO_2 was calcined in NH_3 gas at a temperature of 700 ^oC at a heating rate of 5 ^oC min^{-1} for 60 minutes.

2.3 Synthesis of CC@TiO_xN_y@SnS_2 nanocomposites

SnS_2 nanosheets were decorated on the TiN nanowires by hydrothermal method. A piece of carbon cloth covered uniformly with TiN nanowires was immersed in a solution of Tin(IV) chloride pentahydrate ($SnCl_4{\cdot}5H_2O$, 0.14 g) and L-cysteine (0.77 g), then transferred into a Teflon-lined stainless steel autoclave (50 mL), and hydrothermally treated in an air-flow electric oven at 160 °C for 240 minutes and cooled down to room temperature. A greenish-black CC@TiO_xN_y@SnS_2 film was collected, washed with distilled water and dried for subsequent experiments.

2.4 Synthesis of CC@SnS_2 and SnS_2

Tin(IV) chloride pentahydrate ($SnCl_4{\cdot}5H_2O$, 0.14 g) and L-cysteine (0.77 g) were dissolved in water. A piece of clean carbon cloth was immersed into the solution, transferred into a Teflon-lined stainless steel autoclave. The sealed autoclave was heated in an electric oven at 160 ^oC for 240 minutes and cooled down to room temperature. A green carbon cloth covered with SnS_2 (CC@SnS_2) was collected, washed with water and dried in 60 ^oC. The preparation process of pristine SnS_2 nanosheets was similar to CC@SnS_2, except for adding carbon cloth.

2.5 Material Characterization

The phase, morphology, structure and composition of the as-synthesized samples were characterized by X-ray diffraction (XRD, Bruker, D8 ADVANCE, Cu Kα radiation), field-emission scanning electron microscopy (FE-SEM, JSM-6330F), transmission electron microscopy (TEM, JEM2010-HR, 200 KV), X-ray Photoelectron Spectroscopy (XPS, ESCALab250, Thermo VG) and Raman spectrometer (FT-IR, Nicolet 330).

2.6 Electrochemical Measurement

The electrochemical properties of the samples were tested using CR2032-type coin cells. For pristine SnS_2 nanosheets, the working electrode was composed of active material, carbon black (Super-P-Li), and polyvinylidene fluoride (PVDF) at a weight ratio of 80:10:10. The electrode slurry was coated onto Cu foil and then dried under vacuum at 100 °C over night. For other composition, the working electrodes were prepared by cutting the carbon cloth covered uniformly with samples into smaller square pieces with area of 0.64 cm^2. Both the carbon cloth with loading samples and bare carbon cloth were weighed in a high-precision analytical balance (Sartorius, max weight 5100 mg, *d*=0.001 mg). The mass loading of the active material was 1~2 mg cm^{-2}. The 2032 Coin cells were assembled in an argon-filled glove box [Mikrouna (China) Co., Ltd., the moisture and oxygen concentrations below 1.0 ppm] using a pure lithium foil as the counter and reference electrode, 1 M $LiPF_6$ in a mixture of ethylene carbonate/dimethyl carbonate (1:1, V/V) as electrolyte, and a microporous membrane (Celgard 2400) as the separator. The galvanostatic charge-discharge performances were tested at different current densities in the voltage range of 0.01-3 V using a Neware battery testing system. Cyclic voltammogram (CV) measurements and electrochemical impedance spectroscopy (EIS) measurements were performed with an electrochemical workstation (CHI 760D) at room temperature.

3. Results and Discussion

TiO_xN_y and SnS_2 nanocomposites were grown on carbon cloth by two steps hydrothermal reaction. Firstly, TiN nanowires

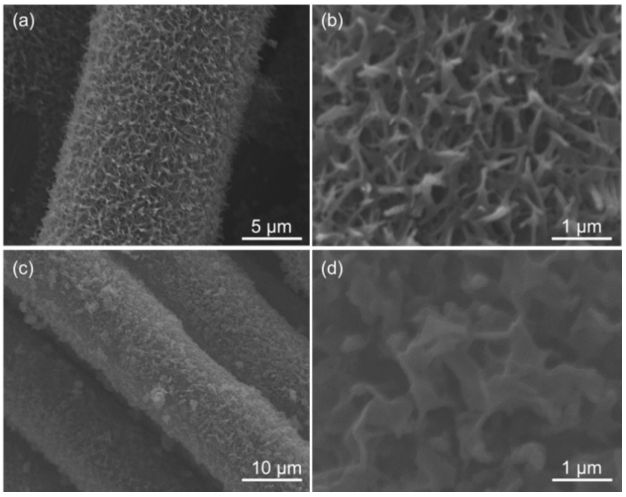

Fig. 1 (a) SEM image of TiN nanowires. (b) Magnified SEM image of the TiN nanowires. (c) SEM image of CC@TiO_xN_y@SnS_2. (d) Magnified SEM image of the CC@TiO_xN_y@SnS_2.

were obtained by growing TiO_2 nanowires on a flexible carbon cloth substrate, followed by further thermal treatment in NH_3 atmosphere. X-ray diffraction (XRD) data confirmed that the TiN nanowires are cubic phase (Fig. S1). In Fig. 1a, SEM image shows that the surface of carbon cloth is uniformly covered with TiN nanowires. The SEM images with a high magnification (Fig. 1b) displays that the TiN nanowires have diameters in a typical range between 100 and 200 nm and lengths about 1.5μm. The as-prepared carbon cloth supported TiN nanowires were then immersed in a solution containing $SnCl_4{\cdot}5H_2O$ and L-cysteine, and hydrothermal reaction heated at 160 ^oC for 240 minutes to form the final products CC@TiO_xN_y@SnS_2. The XRD spectra of the CC@TiO_xN_y@SnS_2 nanocomposites (Fig. S2) shows that the reflections from TiO_2, TiN, SnS_2 and carbon textile can be clearly discerned, which match with the PDF patterns of JCPDS card no. 21-1272 (TiO_2), JCPDS card no. 65-0965 (TiN) and JCPDS card no. 23-0677 (SnS_2), justifying the formation of the CC@TiO_xN_y@SnS_2 nanocomposites.SEM images collected from the CC@TiO_xN_y@SnS_2 nanocomposites are shown in Fig. 1. In Fig. 1c, the surface of the carbon textile also becomes rough, when compared with the bare TiN nanowires (Fig. 1b). The higher magnification SEM image in Fig. 1d reveals that the SnS_2 nanosheets with lateral size of about 300-400 nm are uniformly coated on the TiN nanowires substrate.

The structure of the as-synthesized CC@TiO_xN_y@SnS_2 can be seen clearly in the TEM image in Fig. 2a. The selected-area electron diffraction (SAED) patterns demonstrate that the CC@TiO_xN_y@SnS_2 nanocomposites are polycrystalline in nature (Fig. 2a inset). Well-resolved lattice fringes of 0.31 nm corresponding to the (100) planes of the hexagonal SnS_2 (JCPDS card no. 23-0677) are observed in the nanocomposites (Fig. 2b and 2c), consistent with the layered structure of the SnS_2. Additionally, energy dispersive spectroscopy (EDS) elemental mapping collected from the part of Fig. 2a show that the Sn and S signals are strongly detected, while the Ti, O, N signals are detected to be sparingly distributed in the nano-

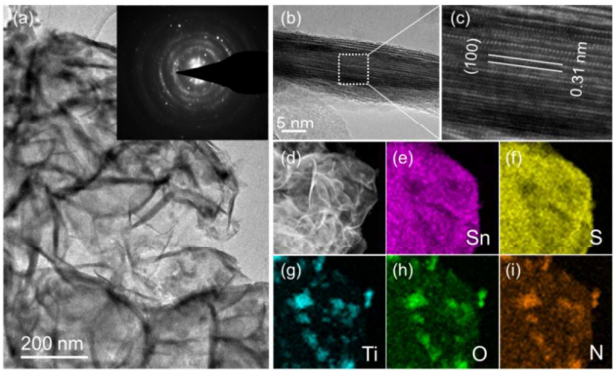

Fig. 2 (a) TEM image of CC@TiO_xN_y@SnS_2, inset image is the SAED pattern. (b) HRTEM and (c) Magnified HRTEM of a single nanosheet. (d - i) EDS elemental mapping images characterized at the same position of the individual elements in the nanosheets.

sheets (Fig. 2d-i). The EDS data reveal that the TiO_xN_y@SnS_2 nanocomposites have the Ti:O:N:Sn:S ratio of 10:15:9:41:25.

For comparison, carbon cloth covered with SnS_2 nanosheets (CC@SnS_2) was also prepared according to the preparation of CC@TiO_xN_y@SnS_2 without the absence of TiN nanowires. All of the XRD peaks can be assigned to layered structure SnS_2 and carbon cloth (Fig. S3) and SEM image certified that the carbon cloth covered by uniform SnS_2 nanosheets (Fig. S4). Also, the pristine SnS_2 samples were synthesized without carbon cloth. The XRD pattern can be assigned to layered structure SnS_2 without other impurity phase (Fig. S3). The SEM image (Fig. S5) illustrates that the pristine SnS_2 has uniform nanosheets morphology.

The full Raman spectra of the CC@TiO_xN_y@SnS_2 nanocomposites are shown in Fig. S6. The enlarge spectrum of the high wavelength region displayed in Fig. 3a shows Raman shift of 146, 441 and 638 cm^{-1} corresponds to the characteristic Raman peaks of TiO_xN_y,[31] while the one at 314 cm^{-1} is assigned to SnS_2 Raman peaks.[32, 33] This further confirms the formation of the CT@TiO_xN_y@SnS_2 nanocomposites. Fig. 3b shows the enlarge Raman spectra of the low Raman shift region, which corresponds to the carbon bonding region. The D and G peaks of the carbon cloth was distorted and some new peaks emanates around 1400-1500 cm^{-1}, which are attributed to the C=N stretching bond, resulted from the reaction of reduced N and carbon cloth.[34, 35] Such C=N bond has been proven to be have high electrical conducti-

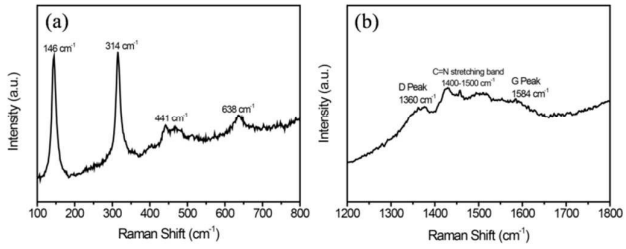

Fig. 3 Enlarged Raman Spectrum of CC@TiO_xN_y@SnS_2: (a) from 100 - 800 cm^{-1} Raman shift, (b) from 1200 - 1800 cm^{-1} Raman shift.

vity, which may enhance the electrical conductivity of the fabricated CT@TiO_xN_y@SnS_2 nanocomposites.[36]

Furthermore, X-ray photoelectron spectroscopy (XPS) studies were carried out to determine the change of surface chemical composition and oxidation state of the CC@TiO_xN_y@SnS_2 nanocomposites. To get the insight study about the oxidation states, the XPS experiment was also performed for the TiN for comparison. Fig. 4a shows the XPS survey spectra of the TiN nanowires and the CC@TiO_xN_y@SnS_2 nanocomposites. The XPS spectra of the CC@TiO_xN_y@SnS_2 nanocomposites consists of mainly the Sn, S, Ti, O, N and C oxidation states; while the no trace of Sn and S peaks can be observed in the TiN spectra. The Ti 2p core-level spectra of the two samples can be seen in Fig. 4b. Multiple peaks are evolved in the Ti 2p spectra of the TiN, which were assigned to be Ti-N, Ti-O-N and Ti-O,[37] but the Ti-N peak was absent in the Ti 2p spectra of the CC@TiO_xN_y@SnS_2 nanocomposites, confirming the formation of the oxynitride.[38, 39] Similar phenomenon can also be observed in the N 1s core-level spectra (Fig. 4c). The N 1s spectrum of the TiN presents a doublet at around 396 and 397 eV, corresponding to the Ti-N and Ti-O-N peaks, respectively; while the Ti-N peak is also not present in the CC@TiO_xN_y@SnS_2 nanocomposites, which also affirms that the oxynitride was formed.[40, 41] These results reveal that the surfaces of the CC@TiO_xN_y@SnS_2 nanocomposites are composed of Ti-O-N and Ti-O chemical states. An additional peak at binding energy of about 164.5 was observed in the S 2p peaks of the CC@TiO_xN_y@SnS_2 nanocomposites, which is quite different from the common S 2p spectra reported for SnS_2 in other literatures.[42, 43] This additional peak can be attributed to sulfoxyanion from the sulfite, suggesting the nanocomposite surface is functionalized by some sulfoxyl groups, which have been also reported to possess good electrical conductivity.[44]

Next, we investigate the electrochemical properties of the CC@TiO_xN_y@SnS_2 nanocomposites as anode material for LIBs.

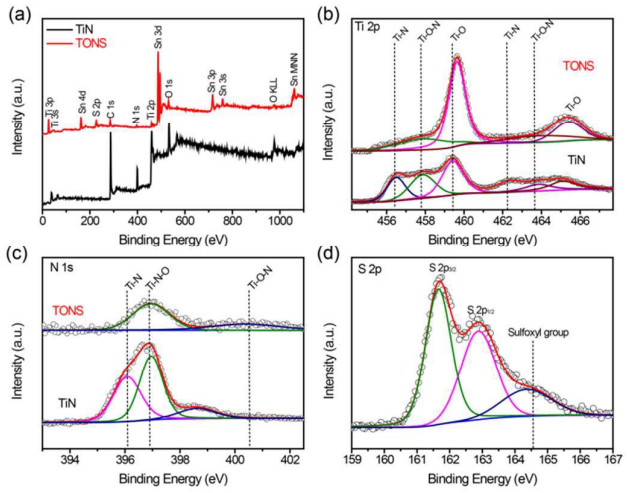

Fig. 4. XPS Characterization of the TiN nanowires and CC@TiO_xN_y@SnS_2 nanocomposites: (a) XPS survey spectrum. (b) Ti 2p core-level spectrum. (c) N 1s core-level spectrum. (d) S 2p core-level spectrum.

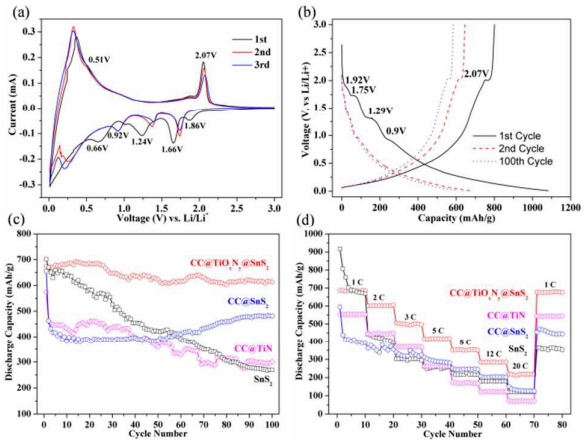

Fig. 5 (a) CV curves of CC@TiO_xN_y@SnS_2 electrode showing the 1st, 2nd and 3rd cycles between 0.01 and 3.0 V at a scanning rate of 0.1 mV/s. (b) The 1st, 2nd and 100th charge-discharge voltage curves of CC@TiO_xN_y@SnS_2 at a current density of 1 C, 1 C = 645 mA g^{-1}. (c) Cyclic performance of CC@TiO_xN_y@SnS_2, CC@TiN, CC@SnS_2 and SnS_2 electrode at a current density of 1 C. (d) Rate capability of CC@TiO_xN_y@SnS_2, CC@TiN, CC@SnS_2 and SnS_2 electrode at various current rates from 1 to 20 C.

Figure 5a shows the 1st-3rd cyclic voltammetry (CV) curves of the CC@TiO_xN_y@SnS_2 nanocomposites between 0.01 and 3.0 V at a scan rate of 0.1 mV s^{-1}. Four reduction peaks can be observed in the 1st CV curve. The peak at 1.86 V is ascribed to the lithium intercalation of the SnS_2 layer without phase decomposition.[18] Two peaks at 1.24 and 0.66 V are attributed to the decomposition of SnS_2 and the formation of Li_2S and Li-Sn alloys.[18] In the subsequent cycles, the reduction peak at 1.24 V can still be observed, and that of 0.66 V shifts to about 0.92 V, which is attributed to form the solid electrolyte interface (SEI) layer. In addition, the redox peaks obtained at 1.66 and 2.07 V are ascribed to the processes of Li^+ insertion and extraction in TiO_2,[8] which is also observed to be highly reversible in subsequent cycles. The CV cures of pristine SnS_2 nanosheets electrode are similar to the CC@TiO_xN_y@SnS_2 nanocomposites expect for the redox peaks obtained at 1.66 and 2.07 V (Fig. S7). Also, the CV cures of CC, CC@SnS_2, and CC@TiN were showed in Fig. S7.

Fig. 5b shows the 1st, 2nd and 100th cycle discharge-charge voltage-capacity curves of the CC@TiO_xN_y@SnS_2 electrode at current density of 1 C. The 1st, 2nd and 100th charge-discharge voltage-capacity curves of CC, SnS_2 nanosheets, CC@SnS_2 and CC@TiN electrode are showed in Fig. S7. From Fig. 5b, it can be seen that four discharge plateaus (ca. 1.97, 1.75, 1.29 and 0.9 V) are apparent at the 1st cycle, which consistent with the results of CV. The initial discharge and charge capacities are 1082 and 800 mAh g^{-1}, corresponding to a coulombic efficiency of 74%, which is considered quite high compared to some SnS_2-based and transition-metal-oxide-based electrodes.[45-47] The first cycle irreversible capacity loss could be attributed to the formation of solid electrolyte interface (SEI) layer. Compared to the total capacity of CC@TiN@SnS_2 electrode, the capacity contribution from the carbon cloth substrate is quite less, even can be ignored (Fig. S7e). The mass loading of the TiO_xN_y@SnS_2 on carbon cloth is 1.6 mg cm^{-2}, the weight

percentage of the TiO_xN_y in CC@TiO_xN_y@SnS_2 is 44 % and SnS_2 is 56 %. Thus, the theoretical capacity of CC@TiO_xN_y@SnS_2 can be calculated as follows: $C_{theoretical}$ = C (TiO_xN_y) × (% mass of TiO_xN_y) + C (SnS_2) × (% mass of SnS_2) = 335 × 44 % + 645 × 56 % = 508.6 mAh g^{-1}. From the second cycle onward, the cycle performance at a current density of 1 C is shown in Fig. 5c. The CC@TiO_xN_y@SnS_2 electrode exhibits excellent capacity retention even prolonging cycle numbers. Apart from the first cycle with a large irreversible capacity, the following up cycles own a coulombic efficiency of about 98% (Fig. S8), a reversible capacity as high as 612 mAh g^{-1} can still be maintained after 100 charging/discharging cycles, which is higher than its theoretical capacity (508.6 mAh g^{-1}). Such capacity is remarkably compared to the previous reports in cycling stability of SnS_2 based electrodes.[16, 18, 19, 48] This capacity is about 1.5 times higher than the theoretical capacity of graphite (372 mAh g^{-1}) and even compared to the theoretical reversible capacity of SnS_2 (645 mAh g^{-1}). For comparison, the cycling performance of CC@TiN, CC@SnS_2 and pristine SnS_2 nanosheets, are also showed in Fig. 5c. Under the same test conditions, the CC@TiN, CC@SnS_2 and pristine SnS_2 nanosheets exhibit much faster capacity fading, after 100 charging/discharging cycles, the discharge capacity are 301, 480 and 270 mAh g^{-1}, respectively. The pristine SnS_2 nanosheets electrode shows the worst cycle performance. Interestingly, the discharge capacity of the CC@TiN@SnS_2 electrode is higher than the addition of individual CC@TiN, CC@SnS_2 and SnS_2 electrode, which is even closed to the theoretical capacity of SnS_2 (645 mAh g^{-1}). After 100 charging/discharging cycles, SEM image of the CC@TiN@SnS_2 electrode studies reveals that the SnS_2 nanosheets still firmly adheres to the surface of the TiO_xN_y nanowires (Fig. S9), indicating that the CC@TiO_xN_y@SnS_2 nanocomposites exhibit excellent chemical stability.

Considering the rate capacity is an important factor for the output powder. The rate capacity of the CC@TiN@SnS_2, CC@TiN, CC@SnS_2 and SnS_2 electrode were carried out by charging/discharging at current density ranging from 1 C to 20 C. As shown in Fig. 5d, the average discharge capacities of CC@TiN@SnS_2 electrode are maintained at 685, 601, 498, 417, 351, 284 and 219 mAh g^{-1} from 1 C to 20 C, respectively. When the current density is switched back to 1 C, a stable high discharge capacity of 676 mAh g^{-1} can be attained. By contract, the discharge capacities of CC@TiN, CC@SnS_2 and SnS_2 electrode drop dramatically with increasing the current density. When compared with CC@SnS_2 and SnS_2 electrode, the CC@TiN@SnS_2 electrode shows higher reversible capacity and better cycling stability. These results clearly demonstrate that the TiO_xN_y play an important role in improving the rate performance of SnS_2.

The attractive electrochemical performance of the CC@TiO_xN_y@SnS_2 electrode might be attributed to the unique structural features in several aspects. First, the flexible carbon cloths substrate, which provides strong mechanical support, acts as a conducting material and current collector. Second, the high electrical conductivity of the TiO_xN_y facilitates the transport of electrons and lithium ions. The link of SnS_2 nano-

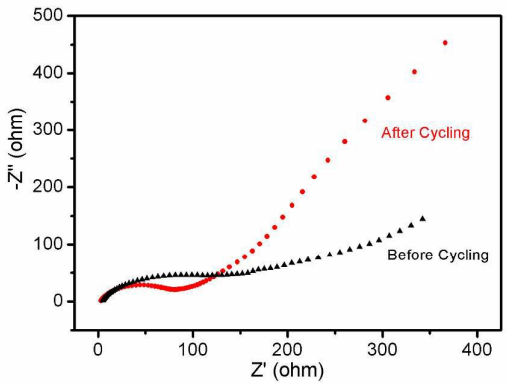

Fig. 6 Nyquist plots of the fresh battery and after 100 charging/discharging cycles of CC@TiO_xN_y@SnS_2 electrode at a current density of 1 C.

sheets and the current collector provides intimate adhesion, ensuring that the active material does not come off from the current collector, and also stimulate electrons transfer between SnS_2 nanosheets and the substrate. Third, the large surface area of the 2D SnS_2 nanosheets with layered structure enhances rapid diffusion of lithium ions. Moreover, the SnS_2 nanosheets anchor on the TiO_xN_y nanowires can allow the electrolyte to penetrate entirely, holding each SnS_2 nanosheet not only surrounded by the electrolyte solution but also contact with the carbon cloth current collector. This is a key feature to high rate capacity. Thus, the above characteristics work together, giving the electrode excellent lithium storage properties.

To deeply understand the electrochemical performances, the electrochemical impedance spectroscopy (EIS) was conducted at room temperature. Fig. 6 shows the Nyquist plots of the fresh and after 100 cycles CC@TiO_xN_y@SnS_2 electrode. Each plot consists of a semicircle in the medium-high frequency region, which is ascribed to the charge transfer or electrochemical reaction resistance, and a sloped line in the low frequency region, which is related to the diffusion of lithium ion. The Nyquist plots exhibit that the diameter of the semicircle for after 100 cycles electrode in the medium-high frequency region is smaller than the fresh electrode, indicating lower charge transfer impedances for after 100 cycles electrode. This phenomenon has been commonly observed for metal oxide LIBs electrodes,[49] and herein could be due to the reduction of the nanocomposite into their corresponding metals during the irreversible reactions.

4. Conclusions

In summary, the novel material CC@TiO_xN_y@SnS_2 nanocomposites were synthesized by two step hydrothermal method. Investigation on the lithium storage performance indicates that the CC@TiO_xN_y@SnS_2 electrode displays an initial discharge capacity of 1082 mAh g^{-1} at a current density of 1 C, with a coulombic efficiency of 74 %. The reversible capacity as high as 612 mAh g^{-1} can still be maintained after 100 cycles charging/discharging. Even at a high current density of 5 C, the electrode shows a high reversible discharge capacity

of 419 mAh g^{-1}. The excellent electrochemical performances suggest that CC@TiO_xN_y@SnS_2 can be feasible alternative electrode materials for the next generation lithium ion batteries. Also, this approach can also be extended for the development of other diverse inorganic electrode materials.

Acknowledgement

This work is supported by Guangxi University of science and technology research projects (KY2015ZD051), Guilin University of Technology research start-up funds (002401003418) and Guilin University of Technology National College Students' Innivation Training Project (201410596003).

References

1 K. Wang and X. Li and J. Chen, *Adv. Mater.*, 2015, **27**, 527-545.
2 M. S. Whittingham, *Chem. Rev.*, 2004, **104**, 4271-4302.
3 J. M. Tarascon and M. Armand, *Nature*, 2001, **414**, 359-367.
4 F. Lu, Q. Wu, X. Yang, L. Chen, J. Cai, C. Liang, M. Wu and P. Shen, *Phys. Chem. Chem. Phys.*, 2013, **15**, 9768-9774.
5 Y. Zhang, Z. Liu, H. Zhao and Y. Du, *RSC Adv.*, 2016, **6**, 1440-1444.
6 C. Jo, Y. Kim, J. Hwang, J. Shim, J. Chun, and J. Lee, *Chem. Mater.*, 2014, **26**, 3508-3514.
7 L. Fan, S. Chi, L. Wang, W. Song, M. He, and L. Gu, *ChemElectroChem* 2015, **2**, 421-426.
8 W. Li, F. Wang, Y. Liu, J. Wang, J. Yang, L. Zhang, A. A. Elzatahry, D. Al-Dahyan, Y. Xia, and D. Zhao, *Nano Lett.*, 2015, **15**, 2186−2193.
9 Y. Huang, C. Ling, X. Chen, D. Zhou and S. Wang, *RSC Adv.*, 2015, **5**, 32505-32510.
10 Y. Liu, H. Kang, L. Jiao, C. Chen, K. Cao, Y. Wang and H. Yuan, *Nanoscale*, 2015, **7**, 1325-1332.
11 J. Ma, D. Lei, X. Duan, Q. Li, T. Wang, A. Cao, Y. Mao and W. Zheng, *RSC Adv.*, 2012, **2**, 3615-3617
12 L. Wang, L. Zhuo, Y. Yu, F. Zhao, *Electrochim. Acta*, 2013, **112**, 439-447.
13 M.-S. Balogun, W. Qiu, J. Jian, Y. Huang, Y. Luo, H. Yang, C. Liang, X. Lu, and Y. Tong, *ACS Appl. Mater. Interfaces*, 2015, **7**, 23205-23215.
14 H. Zhong, G. Yang, H. Song, Q. Liao, H. Cui, P. Shen, and C.-X. Wang, *J. Phys. Chem. C*, 2012, **116**, 9319-9326.
15 Y. Du, Z. Yin, X. Rui, Z. Zeng, X.-J. Wu, J. Liu, Y. Zhu, J. Zhu, X. Huang, Q. Yan and H. Zhang, *Nanoscale*, 2013, **5**, 1456-1459.
16 M. He, L.-X. Yuan and Y.-H. Huang, *RSC Adv.*, 2013, **3**, 3374-3383.
17 S. Y. Liu, X. Lu, J. Xie, G. Cao, T. Zhu, and X. Zhao, *ACS Appl. Mater. Interfaces*, 2013, **5**, 1588-1595.
18 G. Wang, J. Peng, L. Zhang, J. Zhang, B. Dai, M. Y. Zhu, L. Xia and F. Yu, *J. Mater. Chem. A*, 2015, **3**, 3659-3666.
19 D. Kong, H. He, Q. Song, B. Wang, Q.-H. Yang and L. Zhi, *RSC Adv.*, 2014, **4**, 23372-23376.
20 M.-S. Balogun, M. Yu, C. Li, T. Zhai, Y. Liu, X. Lu and Y. Tong, *J. Mater. Chem. A*, 2014, **2**, 10825-10829.
21 X. Wang, X. Lu, B. Liu, D. Chen, Y. Tong and G. Shen, *Adv. Mater.*, 2014, **26**, 4763-4782.
22 G. Zhou, F. Li and H.-M. Cheng, *Energy Environ. Sci.*, 2014, **7**, 1307-1338.
23 Y. Hu and X. Sun, *J. Mater. Chem. A*, 2014, **2**, 10712-10738.
24 H. Gwon, J. Hong, H. Kim, D.-H. Seo, S. Jeon and K. Kang, *Energy Environ. Sci.*, 2014, **7**, 538-551.
25 L. Shen, Q. Che, H. Li and X. Zhang, *Adv. Funct. Mater.*, 2014, **24**, 2630-2637.
26 Y. Qiu, K. Yan, S. Yang, L. Jin, H. Deng and W. Li, *ACS Nano*, 2010, **4**, 6515-6526.
27 J. Liu, S. Tang, Y. Lu, G. Cai, S. Liang, W. Wang and X. Chen, *Energy Environ. Sci.*, 2013, **6**, 2691-2697.
28 D. Zhou, H. Wu, Z. Wei and B.-H. Han, *Phys. Chem. Chem. Phys.*, 2013, 15, 16898-16906.
29 X.-J. Wang, F. Krumeich, M. Wörle, R. Nesper, L. Jantsky and H. Fjellvåg, *Chem. Euro. J.*, 2012, **18**, 5970-5978.
30 X. Lu, M. Yu, G. Wang, T. Zhai, S. Xie, Y. Ling, Y. Tong and Y. Li, *Adv. Mater.*, 2013, **25**, 267-272.
31 B. Subramanian, C. V. Muraleedharan, R. Ananthakumar and M. Jayachandran, *Surf. Coat. Tech.*, 2011, **205**, 5014-5020.
32 J.-G. Kang, G.-H. Lee, K.-S. Park, S.-O. Kim, S. Lee, D.-W. Kim and J.-G. Park, *J. Mater. Chem.*, 2012, **22**, 9330-9337.
33 P. Chen, Y. Su, H. Liu and Y. Wang, *ACS Appl. Mater. Inter.*, 2013, **5**, 12073-12082.
34 A. C. Ferrari, S. E. Rodil and J. Robertson, *Diam. Relat. Mater.*, 2003, **12**, 905-910.
35 P.-N. Wang, N. Xu, Z.-F. Ying, X.-T. Ying, Z.-P. Liu and W.-D. Yang, *Thin Solid Films*, 2001, **382**, 34-38.
36 M. Belmonte, S. M. Vega-Díaz, A. Morelos-Gómez, P. Miranzo, M. I. Osendi and M. Terrones, *J. Euro. Ceram. Soc.*, 2014, **34**, 1097-1104.
37 X. Lu, G. Wang, T. Zhai, M. Yu, S. Xie, Y. Ling, C. Liang, Y. Tong and Y. Li, *Nano Lett.*, 2012, **12**, 5376-5381.
38 J.-G. Kim, D. Shi, K.-J. Kong, Y.-U. Heo, J. H. Kim, M. R. Jo, Y.C. Lee, Y.-M. Kang and S. X. Dou, *ACS Appl. Mater. Inter.*, 2013, **5**, 691-696.
39 Y. Qiu, K. Yan, S. Yang, L. Jin, H. Deng and W. Li, *ACS Nano*, 2010, **4**, 6515-6526.
40 Z. Peng, D. Jia, J. Tang, Y. Wang, Y. Wang, L. Zhang and G. Zheng, *J. Mater. Chem. A*, 2014, **2**, 10904-10909.
41 A. Glaser, S. Surnev, F. P. Netzer, N. Fateh, G. A. Fontalvo and C. Mitterer, *Surf. Sci.*, 2007, **601**, 1153-1159.
42 T. Zhai, X. Lu, Y. Ling, M. Yu, G. Wang, T. Liu, C. Liang, Y. Tong and Y. Li, *Adv. Mater.*, 2014, **26**, 5869-5875.
43 Z. Zhang, C. Shao, X. Li, Y. Sun, M. Zhang, J. Mu, P. Zhang, Z. Guo and Y. Liu, *Nanoscale*, 2013, **5**, 606-618.
44 W. Jiao, N. Li, L. Wang, L. Wen, F. Li, G. Liu and H.-M. Cheng, *Chem. Commun.*, 2013, **49**, 3461-3463.
45 B. Luo, Y. Fang, B. Wang, J. Zhou, H. Song and L. Zhi, *Energy Environ. Sci.*, 2012, **5**, 5226-5230.
46 L. Mei, C. Xu, T. Yang, J. Ma, L. Chen, Q. Li and T. Wang, *J. Mater. Chem. A*, 2013, **1**, 8658-8664.
47 J. Li, P. Wu, F. Lou, P. Zhang, Y. Tang, Y. Zhou and T. Lu, *Electrochim. Acta*, 2013, **111**, 862-868.
48 L. Ji, H. L. Xin, T. R. Kuykendall, S.-L. Wu, H. Zheng, M. Rao, E. J. Cairns, V. Battaglia and Y. Zhang, *Phys. Chem. Chem. Phys.*, 2012, **14**, 6981-6986.
49 J. Luo, J. Liu, Z. Zeng, C. F. Ng, L. Ma, H. Zhang, J. Lin, Z. Shen and H. J. Fan, *Nano Lett.*, 2013, **13**, 6136-6143.

Graphical Abstract

Free-standing CC@TiO_xN_y@SnS_2 nanocomposites were synthesized via two steps hydrothermal process. The flexible additive-free CC@TiO_xN_y@SnS_2 electrode possesses high lithium storage capacity, outstanding cycling stability and excellent rate performance.